Schweizerischer Erdbebendienst
Service Sismologique Suisse
Servizio Sismico Svizzero
Swiss Seismological Service

ETH zürich

SITE CHARACTERIZATION REPORT

SZWD2: Zweisimmen (BE) - Obersimmentaler Heimatmuseum

Manuel Hobiger, Donat Fäh

Last Modification: 22/05/2020

Schweizerischer Erdbebendienst (SED)
Service Sismologique Suisse
Servizio Sismico Svizzero
Servizi da Terratrembels Svizzer

ETH Zürich
Sonneggstrasse 5
8092 Zürich
Schweiz
manuel.hobiger@sed.ethz.ch

Contents

Summary

The free-field strong-motion station SZWD2 was built next to the Obersimmentaler Heimatmuseum in Zweisimmen (BE). We performed a passive seismic array measurement to characterize the soil underneath the station.
The measurements show that the structure beneath the station has an H/V peak at around 20 Hz. The array measurements were analyzed with different techniques, namely 3-component high-resolution FK (HRFK), WaveDec and Spatial Autocorrelation (SPAC). HRFK and WaveDec give similar dispersion curves for Love waves, but the mode attribution for Rayleigh waves is more challenging. The dispersion curves for the fundamental modes of both Love and Rayleigh waves are retrieved from around 4.1 to 15.4 Hz and 2.4 to 22.4 Hz, respectively.
The joint inversion of Love and Rayleigh wave dispersion curves and the Rayleigh wave ellipticity angle showed that the structure can be explained by two shallow layers at the surface with shear-wave velocities from 130 to 245 m/s, followed by layers with velocities increasing from over 800 m/s to over 2200 m/s at about 200 m depth. The V_{S30} of the best models is about 700 m/s, corresponding to soil class B in both EC8 and SIA261.

1 Introduction

In the framework of the second phase of the Swiss Strong Motion Network (SSMNet) renewal project, a new station was planned in Zweisimmen (BE) as replacement of the old seismic station SZWD, which was operational since 3 December 1993.
The new station is located close to the Obersimmentaler Heimatmuseum, about 210 m southeast of the old station. The new station, called SZWD2, went operational on 8 August 2017. The location of the station is shown in Fig. 1. The location of the old station SZWD is included in the geological map (see Fig. 2).

Figure 1: Map showing the location of station SZWD2 in Zweisimmen. ©2020 swisstopo (JD100042)

2 Geological setting

A geological map of the surroundings of station SZWD2 is shown in Fig. 2. According to the geological atlas, station SZWD2, the old station SZWD and all stations of the passive array measurement lie on moraine.

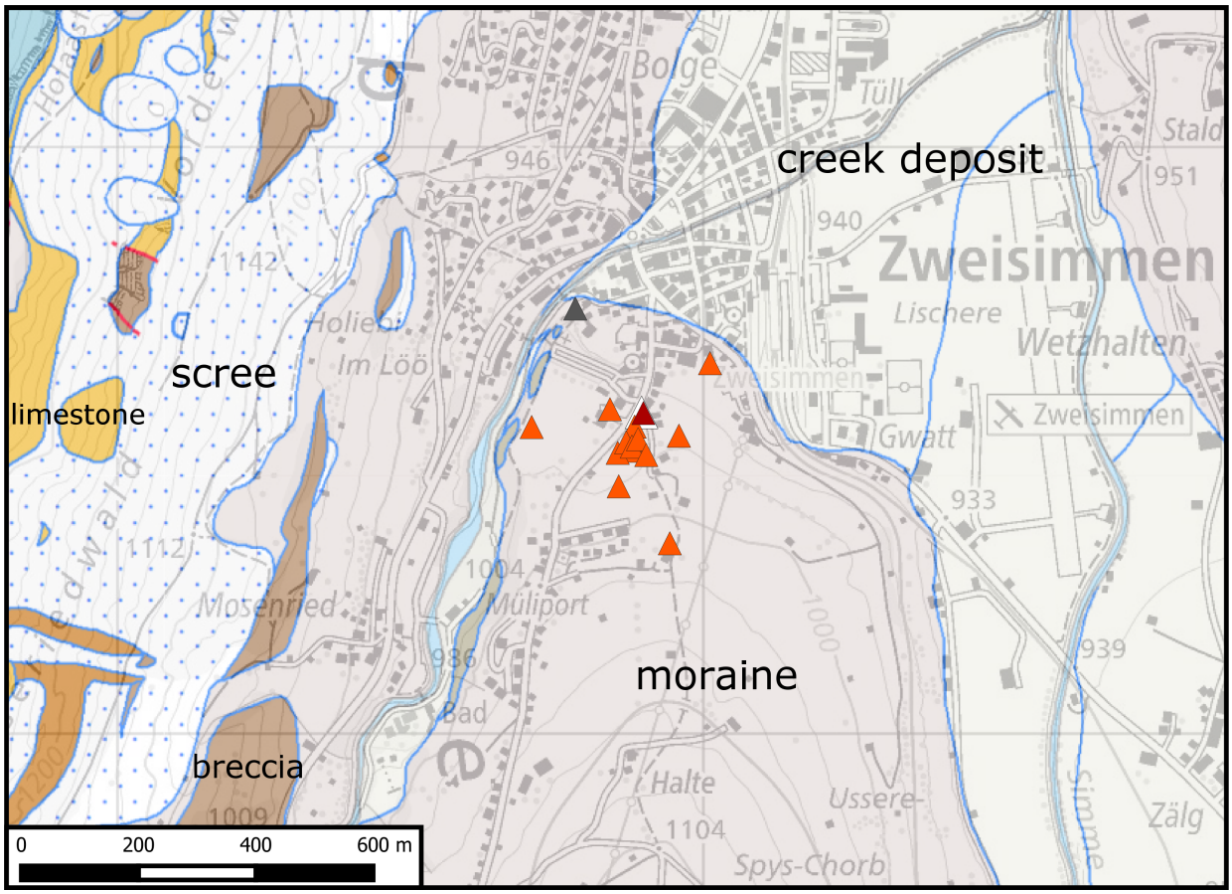

Figure 2: Geological map of the area around station SZWD2 (white triangle) with the different stations of the array measurement (orange triangles and red triangle) and the old station SZWD (gray triangle). ©2019 swisstopo (JD100042)

3 Site characterization measurements

3.1 Data set

In order to characterize the local underground structure around station SZWD2, a passive seismic array measurement was carried out on 25 October 2017. The layout of the array is shown in Fig. 3.
A single array measurement was performed. The array consisted of 16 stations. It was planned to consist of five rings of three stations each around a central station, which was located close to station SZWD2. The ring radii were planned to be 4.8 m, 12 m, 30 m, 75 m, and 180 m, respectively. The final minimum and maximum inter-station distances in the array were 4.7 m and 323.0 m, respectively. The names of the stations of the array are composed of "SZWD" followed by a two-digit number (42 to 49, 52 to 55, 62, 64, 68, 69). The seismic stations consisted of Lennartz 3C 5 s sensors connected to Centaur digitizers. A total of 12 digitizers were used. Twelve sensors were connected to the A channels of the digitizers and another four sensors were connected to B channels. The total recording time was 160 minutes.
The station locations have been measured by a differential GPS system (Leica Viva GS10) which was set up to measure with a precision better than 5 cm. This precision was achieved for all stations.
The array lies on a slope. The northeasternmost station was installed at an elevation of 947 m, the southeasternmost one at 1009 m. All other stations were installed at elevations between 967 and 980 m. Therefore, we neglected slope effects during the array analysis.
As the permanent station SZWD2 was located inside the array, but no array station was located close to it, we performed an additional H/V measurement at a station called ZWE101 next to the permanent station during the dismantling of the array.

Figure 3: Layout of the array measurements around station SZWD2. The location of SZWD2 is indicated by the white triangle, the locations of the stations for the passive seismic measurement by the orange triangles. The red triangle indicates the location of the additional H/V measurement point ZWE101. ©2020 swisstopo (JD100042)

3.2 H/V and RayDec ellipticity curves

Figure 4 shows the H/V curves determined with the time-frequency analysis method (Fäh et al., 2009) for all stations of the passive array. All curves are very similar below 2 Hz, where only the amplitude varies slightly, and show a first peak at about 0.7 Hz. At higher frequencies, most stations show peaks at various frequencies, indicating small-scale near-surface heterogeneities.
The RayDec technique (Hobiger et al., 2009) is supposed to eliminate the contributions of other wave types than Rayleigh waves and give a better estimate of the ellipticity than the classical H/V technique. The RayDec ellipticity curves for all stations of the array measurement are shown in Fig. 4 and are similar to the H/V curves. The curve of station ZWE101 is rather flat between 0.5 and 10 Hz, with a broad peak between 0.5 and 2 Hz.

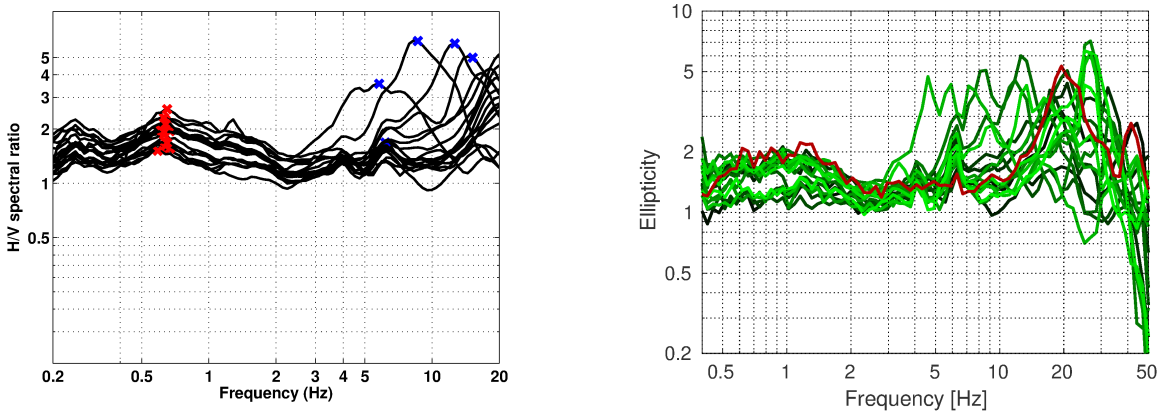

Figure 4: Left: Overview of the H/V measurements for all measurement stations. Right: RayDec ellipticities for all measurement stations. The red curve corresponds to ZWE101, the station close to SZWD2.

3.3 Polarization analysis

The polarization analysis was performed according to Burjánek et al. (2010) and Burjánek et al. (2012). The results for all stations of the array are similar. Only the results for ZWE101 are shown here.
There is no preferential linear particle polarization visible and we do not see indications for 2-dimensional polarization effects.

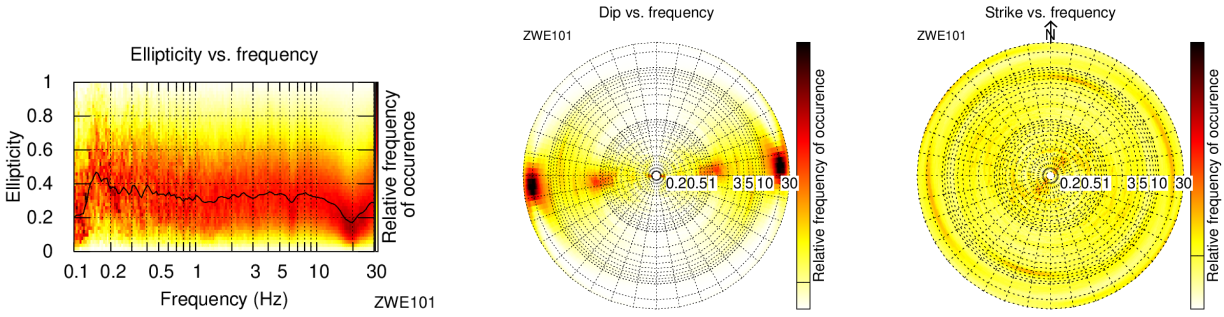

Figure 5: Polarization analysis of station ZWE101.

3.4 SPAC

The SPAC (Aki, 1957) curves of the vertical components have been calculated using the M-SPAC (Bettig et al., 2001) technique implemented in geopsy (Wathelet et al., 2005). Rings with different radius ranges had been defined previously and for all station pairs with distance inside this radius range, the cross-correlation was calculated over a wide frequency range. These cross-correlation curves are averaged for all station pairs of the respective ring and give the SPAC curves. The rings are defined in such a way that at least three station pairs contribute and their connecting vectors have a good directional coverage.
The SPAC curves for all defined rings are shown in Fig. 6. The black points indicate the data values which contributed to the final dispersion curve estimation, which was made with the function `spac2disp` of the geopsy package.
Using SPAC, we can retrieve a Rayleigh wave dispersion curve between 2.3 and 19.1 Hz.

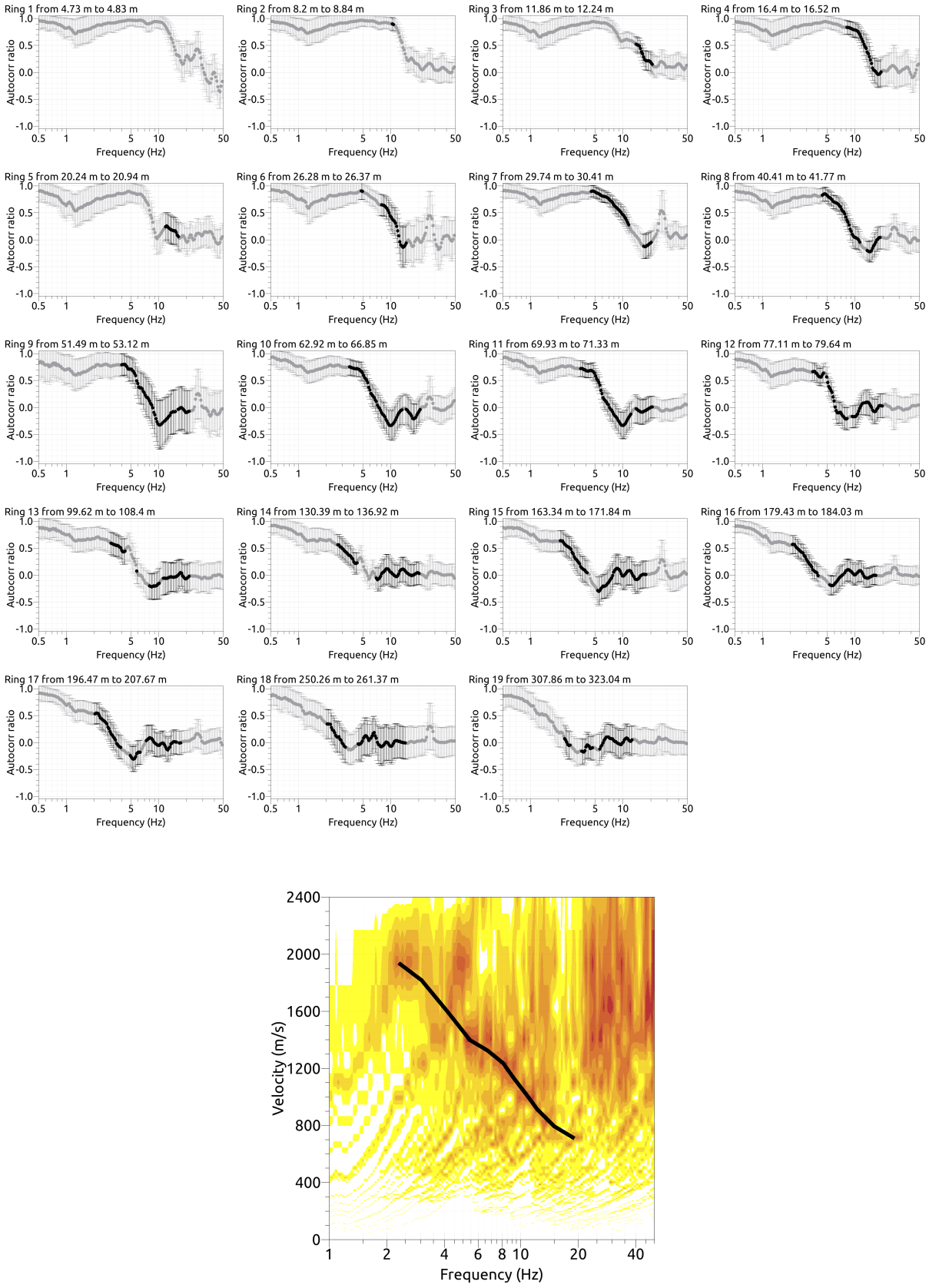

Figure 6: Top: SPAC curves for the different distance ranges. The black data points contributed to the dispersion curve estimation. Bottom: Resulting Rayleigh wave velocities. The black line corresponds to the picked dispersion curve.

3.5 3-component high-resolution FK

The results of the 3-component high-resolution FK analysis (Poggi and Fäh, 2010) are shown in Fig. 7. On the transverse component, corresponding to Love waves, we can clearly identify a dispersion curve between 4.0 and 20.2 Hz, without reaching the high-frequency array resolution limit.
On the vertical component, corresponding to Rayleigh waves, we can clearly identify one mode between 4.6 and 23.3 Hz, also without reaching the high-frequency resolution limit. On the radial component, also related with Rayleigh waves, the results are less clear, but we can pick two dispersion curves between 5.3 and 28.8 Hz and between 10.6 and 21.7 Hz, respectively.
The corresponding ellipticity curves of these modes are mainly flat and show a wide peak around 20 Hz.

3.6 WaveDec

The results of the WaveDec (Maranò et al., 2012) processing are shown in Fig. 8. This technique estimates the properties of single or multiple waves simultaneously with a maximum likelihood approach. In order to improve the results, the parameter γ, which modifies the sharpness of the wave property estimation, has been tuned. Here, a value of $\gamma = 0.2$ was used, corresponding to a predominantly maximum likelihood estimation. The Love wave dispersion curve is not smooth and can be picked from 5.4 to 13.3 Hz. Small parts of a higher mode are visible around 25 Hz.
For Rayleigh waves, the result looks less clear. We can pick two dispersion curves, the first between 5.2 and 11.8 Hz and the second between 4.7 and 12.3 Hz. Both curves are not well separated. For the first one, the ellipticity angle is negative in the whole picked frequency range, indicating retrograde particle motion. For the second one, the ellipticity angle is positive, indicating prograde particle motion. This suggests that the first curve belongs to the fundamental and the second to the first higher mode.

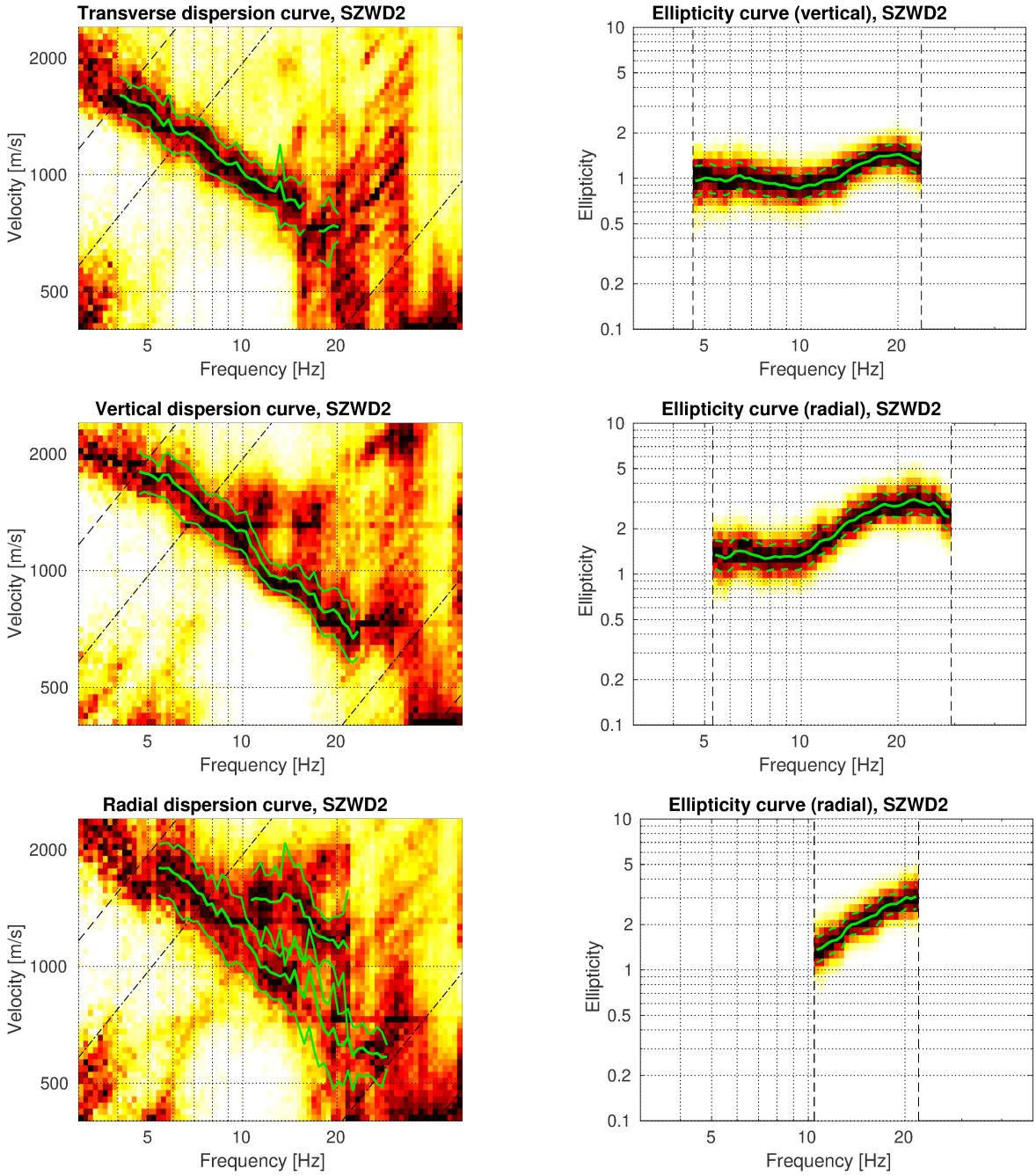

Figure 7: Dispersion and ellipticity curves obtained with the 3-component HRFK algorithm (Poggi and Fäh, 2010). In the left column, the dispersion curves for the transverse, vertical and radial components are shown, and in the right column the ellipticity curves corresponding to the dispersion curves picked on the vertical and radial components. The dashed and dotted black lines are the array resolution limits. The solid green lines are picked from the data, where the central line indicates the best values and the two outer lines the standard deviation.

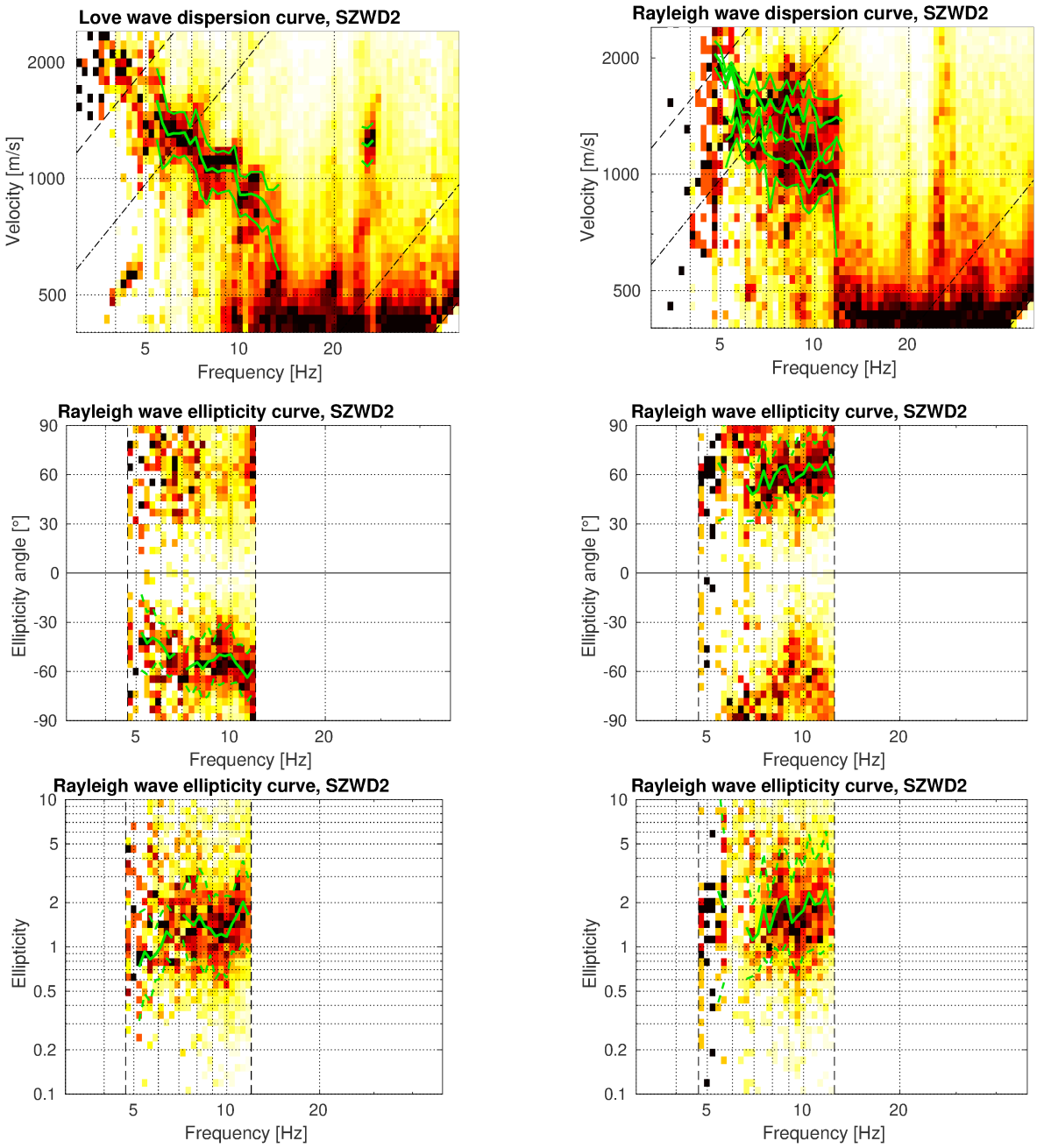

Figure 8: Top: Love (left) and Rayleigh (right) wave dispersion curves obtained with the WaveDec technique (Maranò et al., 2012). The dashed lines indicate the theoretical array resolution limits. Center: Rayleigh wave ellipticity angle curves for the two picked dispersion curves. Bottom: Rayleigh wave ellipticity curves, i.e. the absolute value of the tangent of the ellipticity angle curves shown above.

3.7 Summary

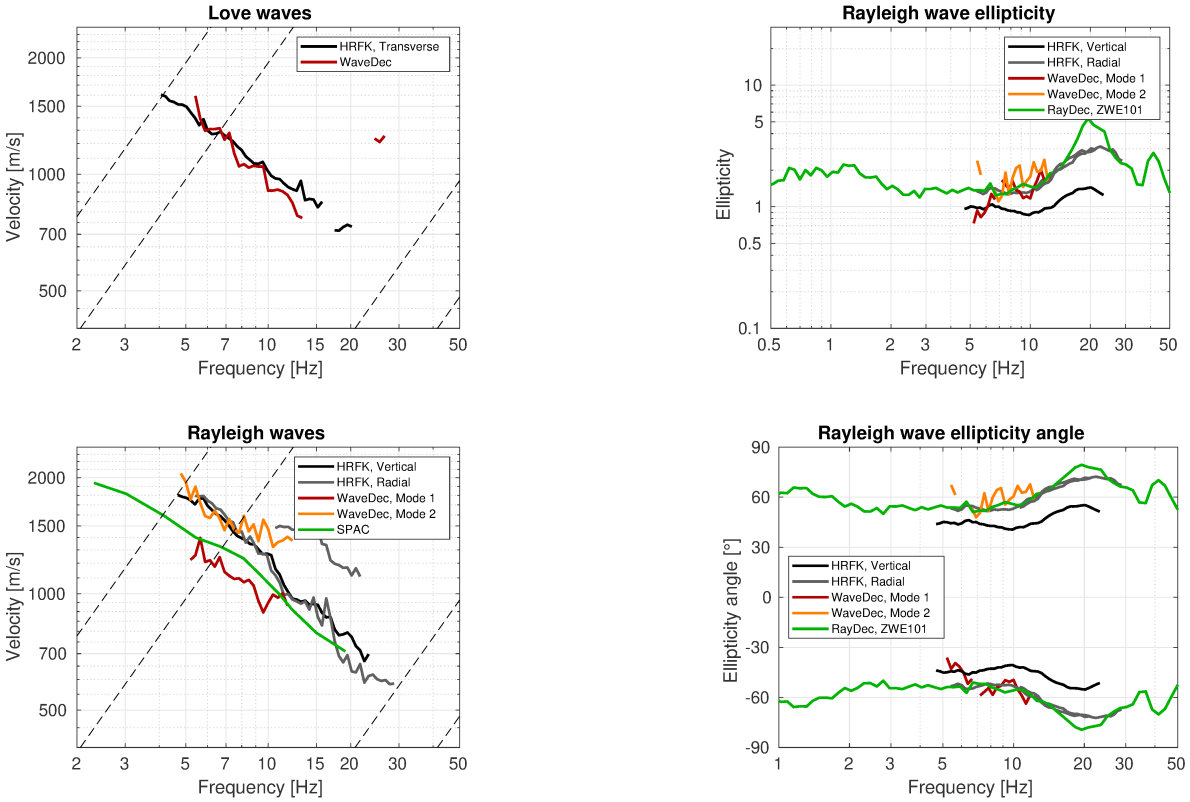

Figure 9: Overview of the Love and Rayleigh wave dispersion curves as well as the ellipticity and ellipticity angle curves for both arrays. The dashed lines indicate the theoretical resolution limits of the array. The RayDec ellipticity curve corresponds to station SZWD244.

Fig. 9 gives an overview of the dispersion and ellipticity curves determined by the different methods.
For Love waves, the HRFK and WaveDec results are in good agreement, the HRFK curve is smoother.
For Rayleigh waves, there are differences for the different modes. The HRFK curves for the vertical and radial components are in good agreement, a higher mode is visible on the radial component. The HRFK curves are in good agreement with the second mode picked for WaveDec for frequencies below 10 Hz. The first picked WaveDec mode shows lower velocities and seems to be in agreement with the HRFK modes above 10 Hz, even if it was not possible to pick it in this frequency range. The SPAC curve lies between the different modes of the other methods and can be a mixture of them. It reaches much lower frequencies. If the WaveDec result with the two modes is correct, it remains questionable why HRFK does not retrieve the fundamental mode below 10 Hz. In any case, the HRFK curves were clearer to pick than the WaveDec curves.
The ellipticity curves retrieved using the different methods are in qualitative agreement as all methods are relatively flat up to 10 Hz and show a peak at around 20 Hz. The single-station ellipticity curve determined with RayDec also covers frequencies lower than 3 Hz. It was transformed to ellipticity angle using the arctangent function. As we cannot distinguish between prograde and retrograde particle motion with a single-station method, we account for both possibilities and the RayDec (and HRFK) curves

are represented twice, once for each sense of rotation. The two WaveDec modes show very similar absolute ellipticity curves, but the angles have opposite sign. The first mode is retrograde in the recovered frequency range and the second mode prograde. This is compatible with the interpretation of the first mode as the fundamental mode and the second as the first harmonic mode. The ellipticity peak at around 20 Hz is not resolved by WaveDec, so it is not completely clear if it is a singularity with change of the sense of rotation or not. The high vales of the peak, however, can be seen as an indication for a singularity.

4 Data inversion

4.1 Inversion targets

Two different inversion targets are defined. For target 1, the vertical HRFK dispersion curve was interpreted as fundamental mode Rayleigh wave dispersion curve. For the second target, the WaveDec interpretation was trusted, but, instead of the WaveDec curve, the SPAC curve, which was close and reaches much smaller frequencies, was used as fundamental mode for frequencies below 10 Hz. At higher frequencies, the HRFK curve was used. As the SPAC curve was picked without uncertainty estimation, a realistic estimation was used (as can be seen in Fig. 10). In both targets, the transverse HRFK curve was used as Love wave dispersion curve. The RayDec curve was transformed into ellipticity angle representation and used as fundamental mode ellipticity. The peak at around 20 Hz was assumed to be a singularity and the particle motion below was assumed to be retrograde and prograde above, using negative and positive ellipticity angles, respectively. The details of the inversion targets are indicated in Tables 1 and 2 and the corresponding curves are shown in Fig. 10.

Table 1: List of the different data curves used as inversion target 1.

Method	Wave type	Mode	Curve type	Frequency range [Hz]
HRFK (T)	Love	fundamental	dispersion	4.06 - 15.4
HRFK (V)	Rayleigh	fundamental	dispersion	4.80 - 22.4
RayDec (ZWE101)	Rayleigh	fundamental	ellipticity angle (-)	2.09 - 18.2
RayDec (ZWE101)	Rayleigh	fundamental	ellipticity angle (+)	23.3 - 35.4

Table 2: List of the different data curves used as inversion target 2.

Method	Wave type	Mode	Curve type	Frequency range [Hz]
HRFK (T)	Love	fundamental	dispersion	4.06 - 15.4
SPAC	Rayleigh	fundamental	dispersion	2.37 - 9.34
HRFK (V)	Rayleigh	fundamental	dispersion	11.98 - 22.4
RayDec (ZWE101)	Rayleigh	fundamental	ellipticity angle (-)	2.09 - 18.2
RayDec (ZWE101)	Rayleigh	fundamental	ellipticity angle (+)	23.3 - 35.4

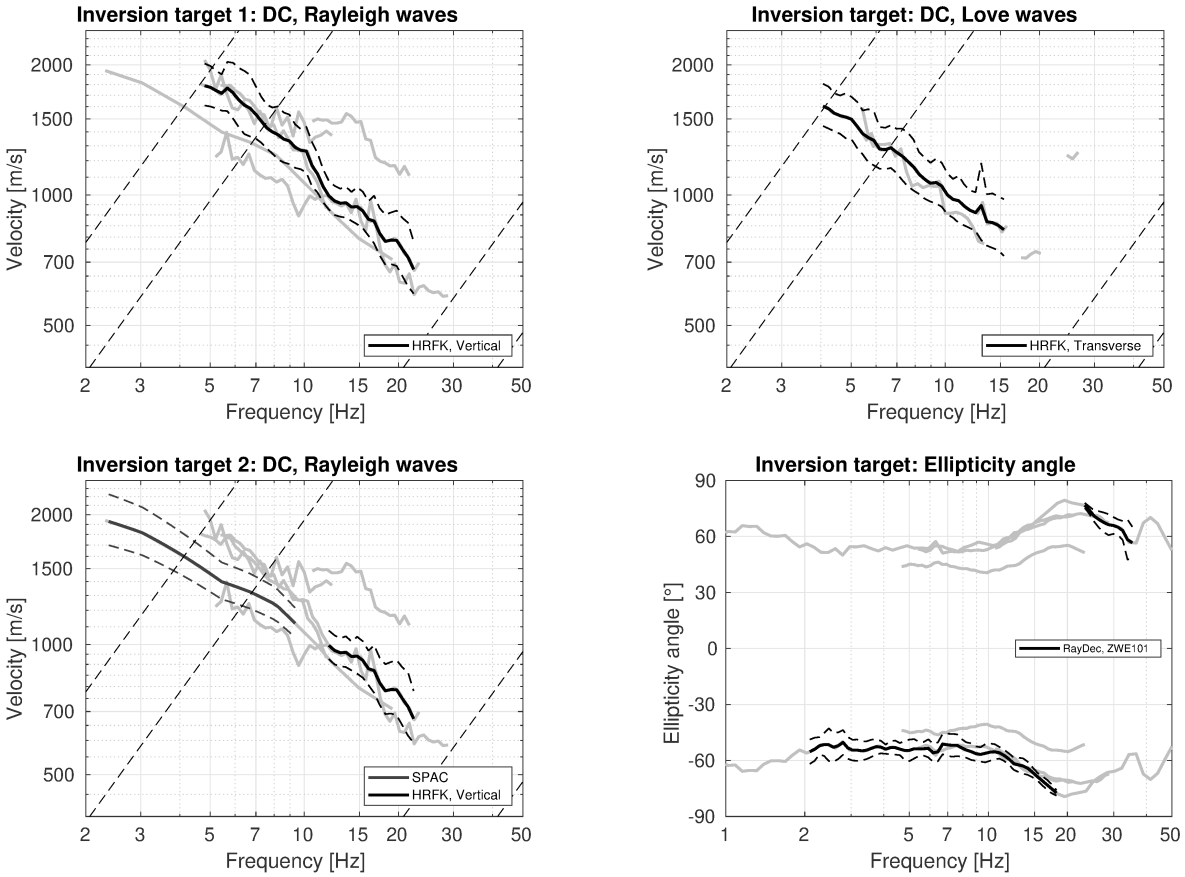

Figure 10: Overview of the dispersion and ellipticity angle curves used as targets for the different inversions.

4.2 Inversion parameterization

Six different parameterizations have been used in total. The first five had free values of the depths and velocities of the different layers, ranging from four to eight layers (including the half-space). The last parameterization had fixed layer depths and consisted of 20 layers in total. The P-wave velocities were allowed to vary up to 5000 m/s. The S-wave velocities were allowed to range from 30 to 3500 m/s. The deepest layers were parameterized to reach a depth of 200 m maximum. The density was fixed to 2 300 kg/m^3 for the lowest layer, to 1 900 kg/m^3 for the superficial layer (or the first three layers in the fixed-layer case) and to 2 100 kg/m^3 for all other layers. No low-velocity zones were allowed.

4.3 Inversion results

We performed inversions with six different parameterizations for each of the two targets. In Table 3, the obtained minimum misfit values for these inversions are shown. Each inversion run produced around 150 000 total models in order to assure a good convergence of the solution. The results of the inversions SZWD4l1 to SZWDfix1, using target 1, are shown in Figs 11 - 16. The results of the inversions with target 2 are shown in Figs 17 - 22. The different inversions for the respective targets yield similar misfit values and fit the data in a comparable way. The 4-layer inversions yield higher misfit values than the other inversions, the 5-layer inversions have slightly higher misfit values. For the inversions with target 1, the misfits are higher than for target 2, because the assumed measurement errors for the SPAC dispersion curve were larger than for the HRFK curve.

Table 3: List of inversions

Inversion	Target	Number of layers	Number of models	Minimum misfit
SZWD4l	1	4	150 023	0.529
SZWD5l	1	5	150 021	0.432
SZWD6l	1	6	150 065	0.400
SZWD7l	1	7	150 057	0.397
SZWD8l	1	8	149 998	0.412
SZWDfix	1	20	150 002	0.387
SZWD4l2	2	4	150 025	0.491
SZWD5l2	2	5	150 016	0.360
SZWD6l2	2	6	150 017	0.313
SZWD7l2	2	7	150 088	0.333
SZWD8l2	2	8	150 012	0.355
SZWDfix2	2	20	150 076	0.354

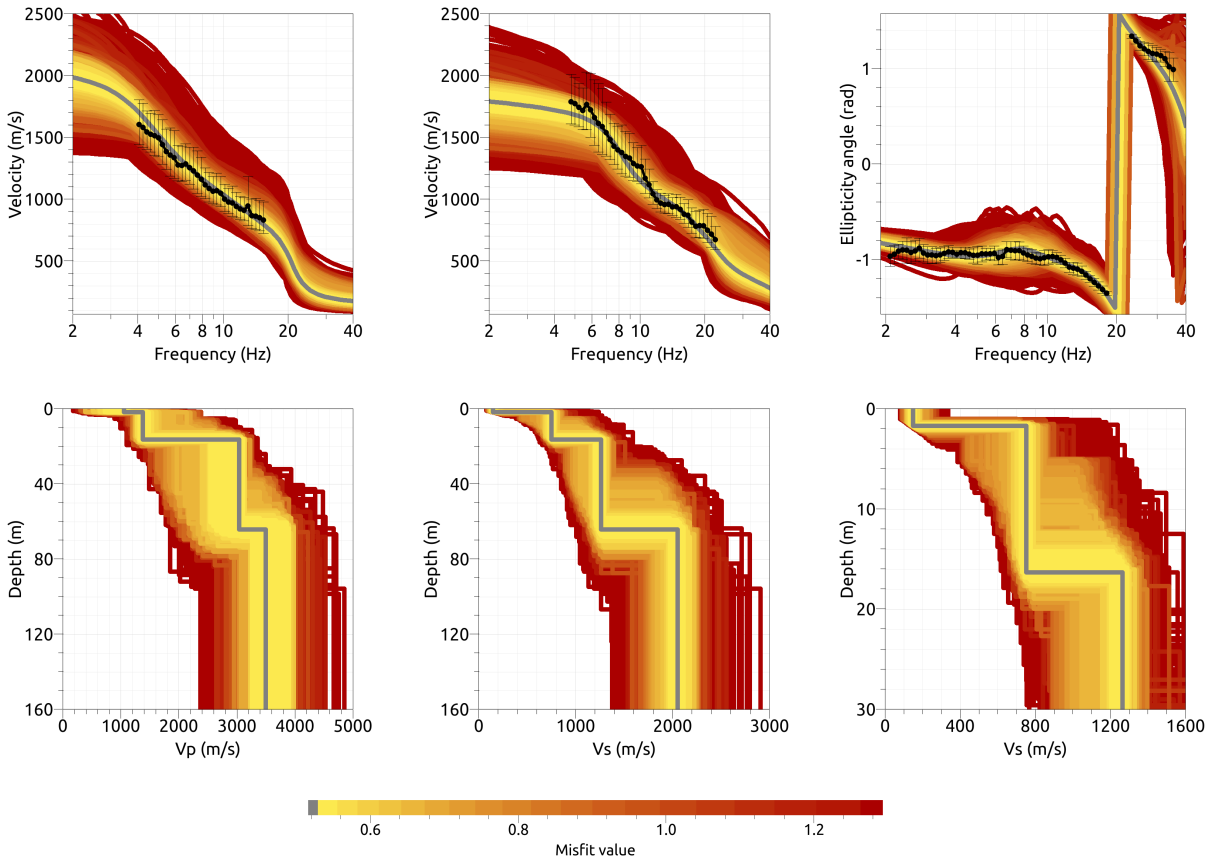

Figure 11: Inversion SZWD4l. Top line: Dispersion curves for Love waves (left) and Rayleigh waves (center) and Rayleigh wave ellipticity angle (right) of the respective fundamental modes. Bottom line: P-wave velocity profiles (left), S-wave velocity profiles (center and zoom on the right). The black dots indicate the data points used for the inversion, the gray line indicates the best-fitting model.

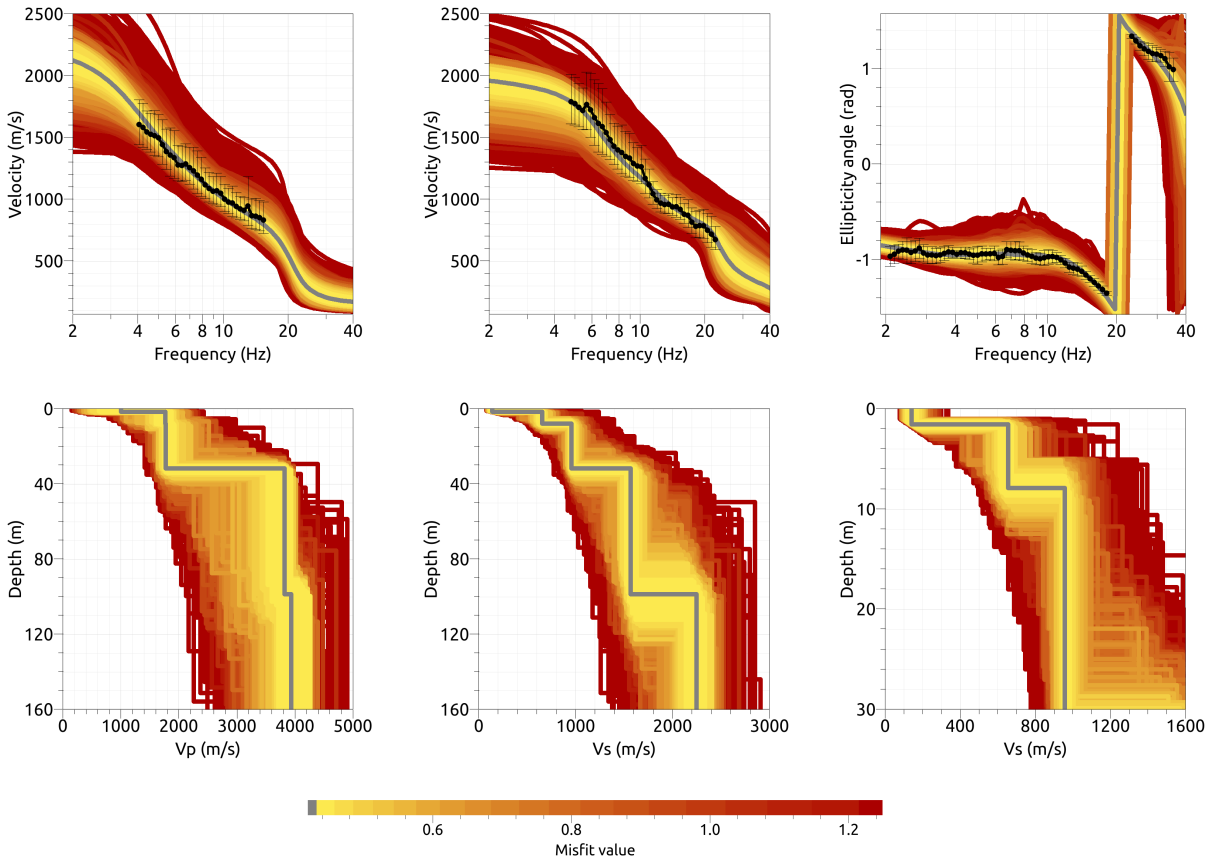

Figure 12: Inversion SZWD5l. Top line: Dispersion curves for Love waves (left) and Rayleigh waves (center) and Rayleigh wave ellipticity angle (right) of the respective fundamental modes. Bottom line: P-wave velocity profiles (left), S-wave velocity profiles (center and zoom on the right). The black dots indicate the data points used for the inversion, the gray line indicates the best-fitting model.

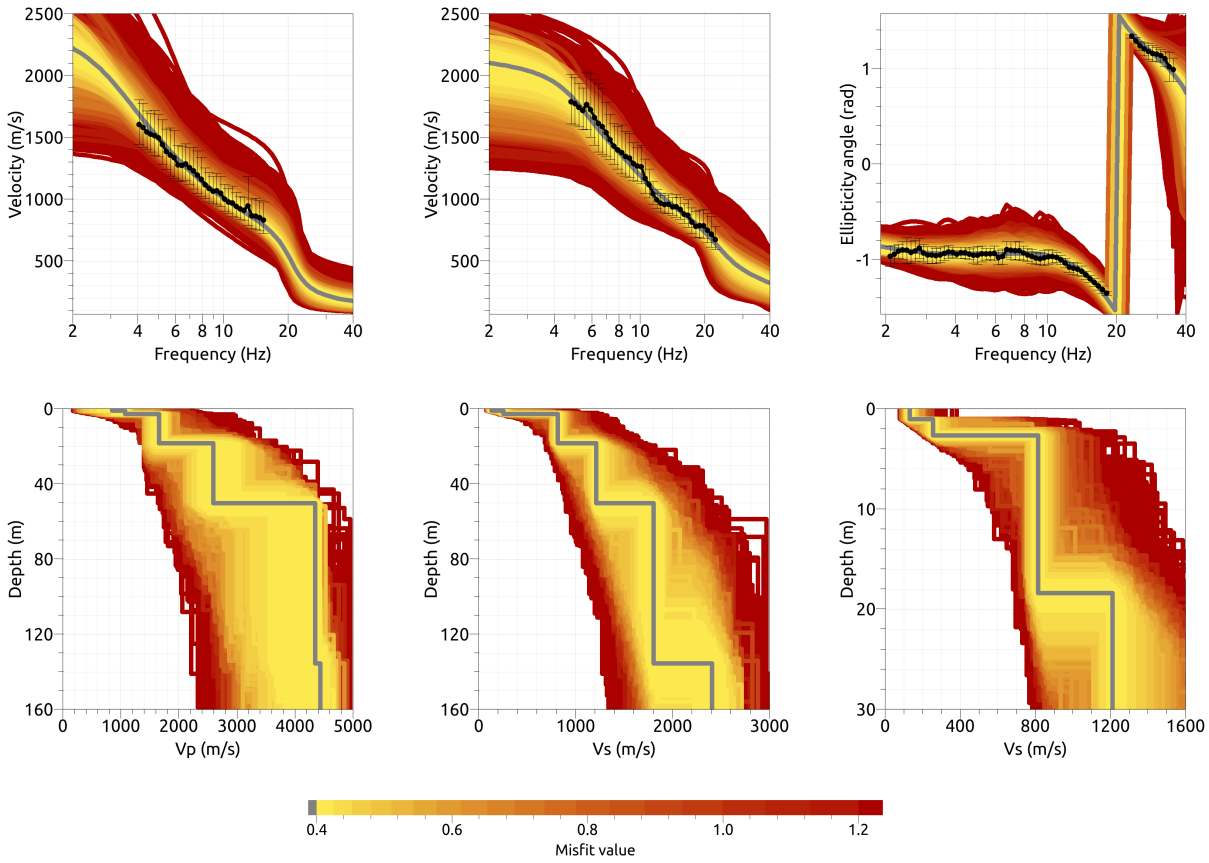

Figure 13: Inversion SZWD6l. Top line: Dispersion curves for Love waves (left) and Rayleigh waves (center) and Rayleigh wave ellipticity angle (right) of the respective fundamental modes. Bottom line: P-wave velocity profiles (left), S-wave velocity profiles (center and zoom on the right). The black dots indicate the data points used for the inversion, the gray line indicates the best-fitting model.

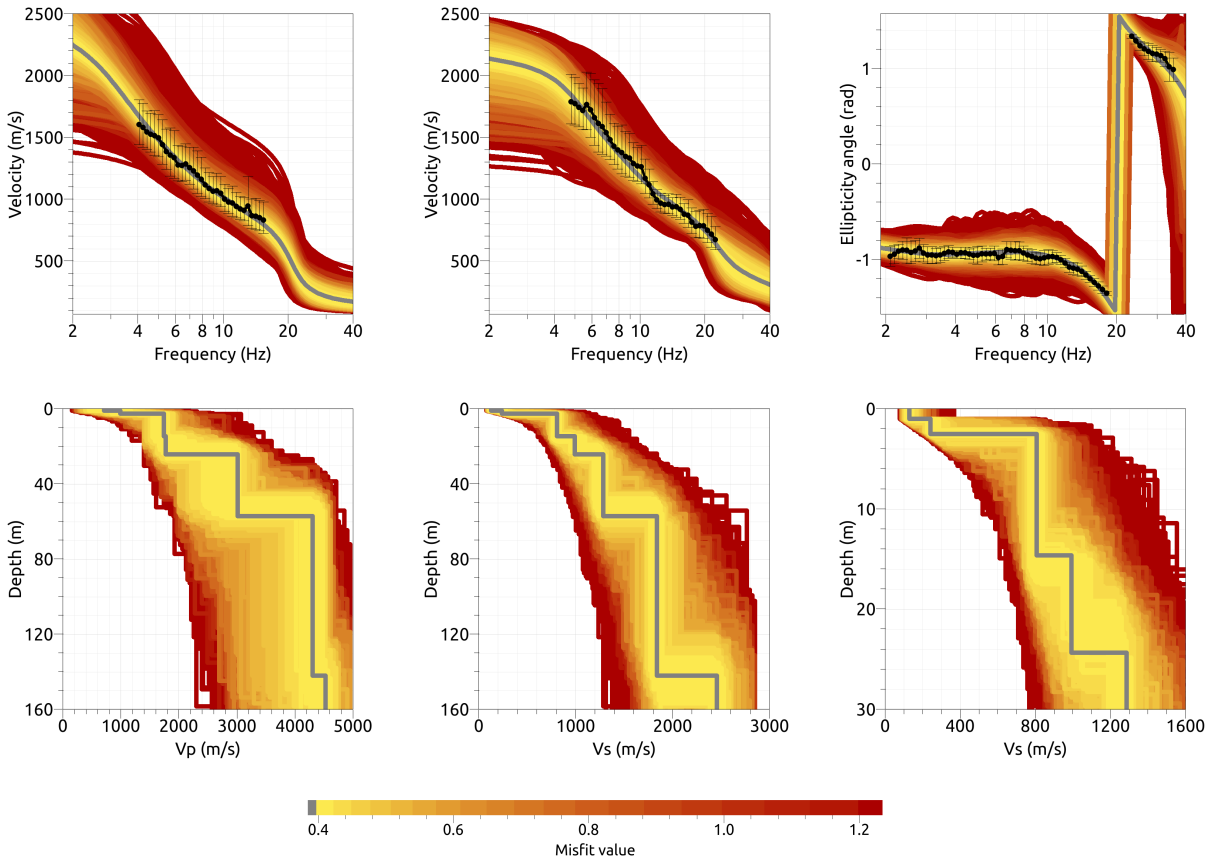

Figure 14: Inversion SZWD7l. Top line: Dispersion curves for Love waves (left) and Rayleigh waves (center) and Rayleigh wave ellipticity angle (right) of the respective fundamental modes. Bottom line: P-wave velocity profiles (left), S-wave velocity profiles (center and zoom on the right). The black dots indicate the data points used for the inversion, the gray line indicates the best-fitting model.

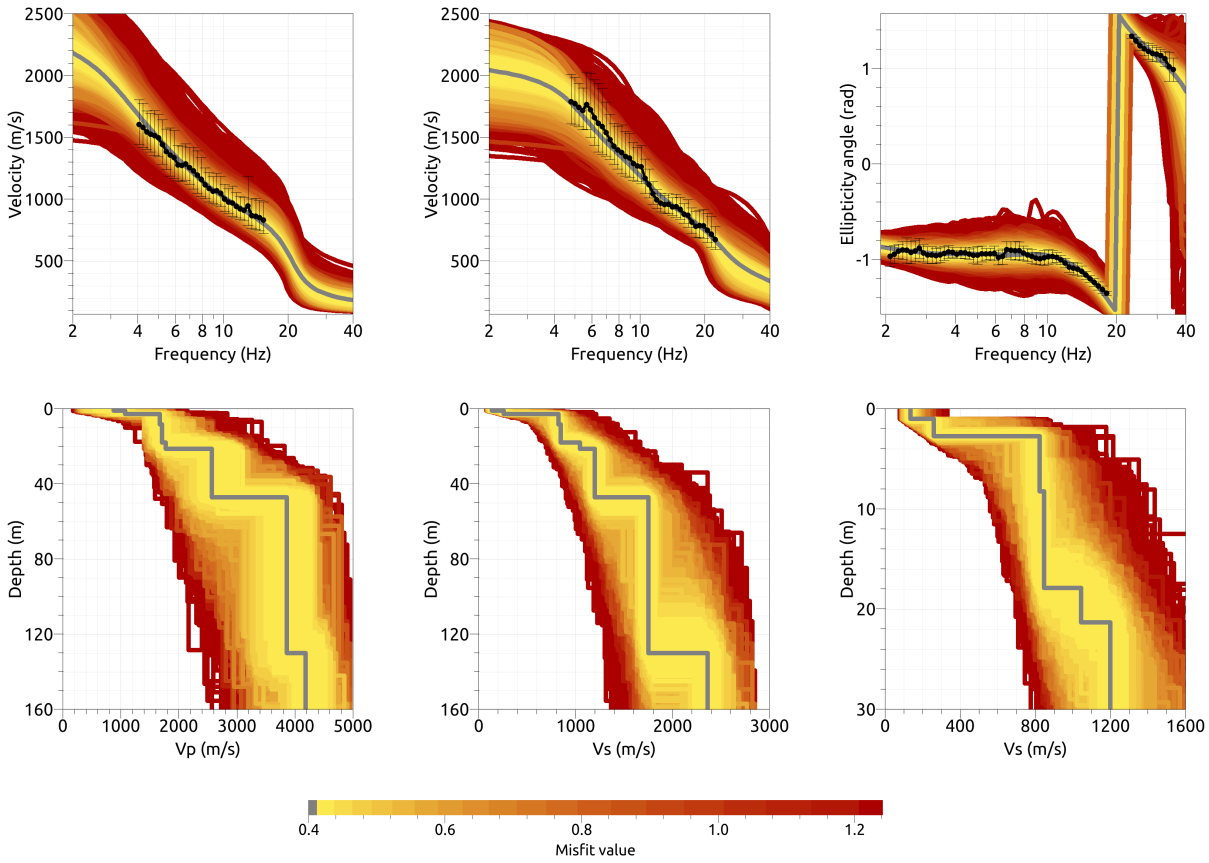

Figure 15: Inversion SZWD8l. Top line: Dispersion curves for Love waves (left) and Rayleigh waves (center) and Rayleigh wave ellipticity angle (right) of the respective fundamental modes. Bottom line: P-wave velocity profiles (left), S-wave velocity profiles (center and zoom on the right). The black dots indicate the data points used for the inversion, the gray line indicates the best-fitting model.

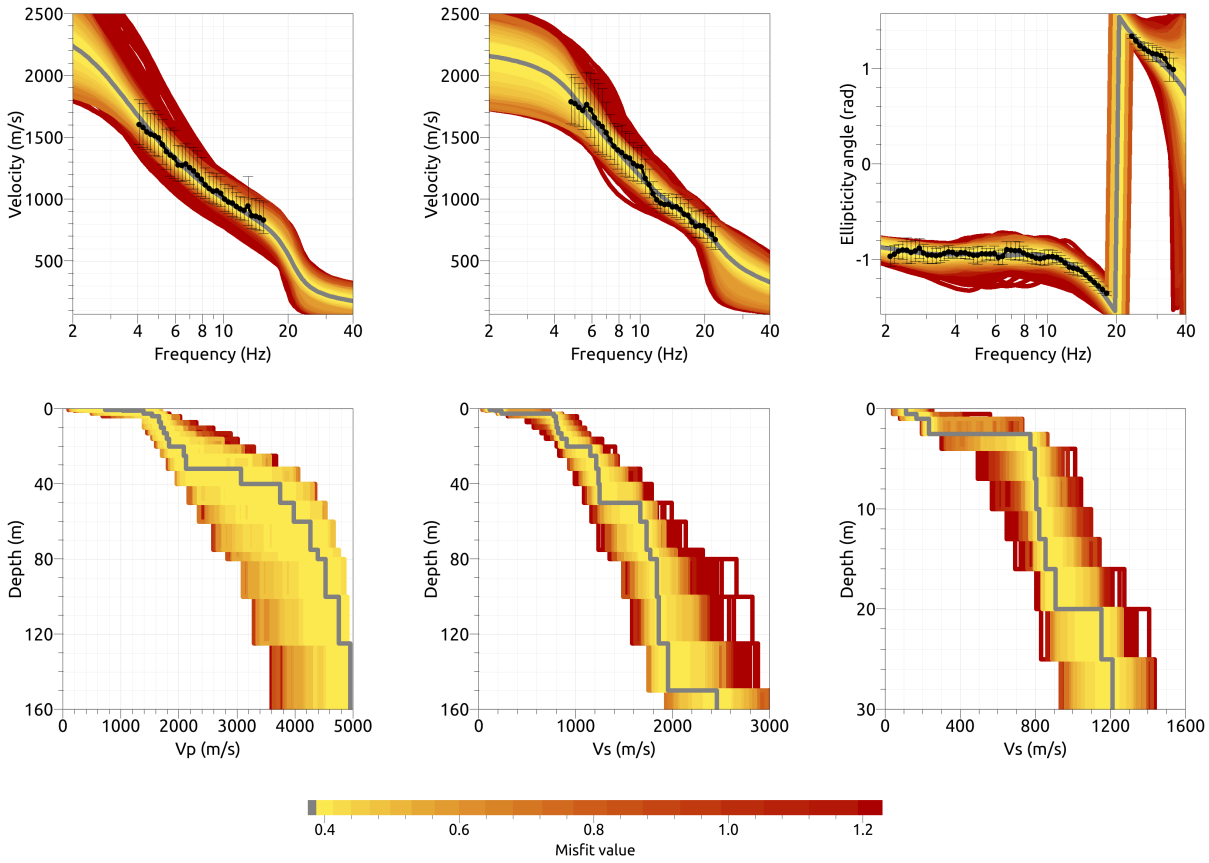

Figure 16: Inversion SZWDfix. Top line: Dispersion curves for Love waves (left) and Rayleigh waves (center) and Rayleigh wave ellipticity angle (right) of the respective fundamental modes. Bottom line: P-wave velocity profiles (left), S-wave velocity profiles (center and zoom on the right). The black dots indicate the data points used for the inversion, the gray line indicates the best-fitting model.

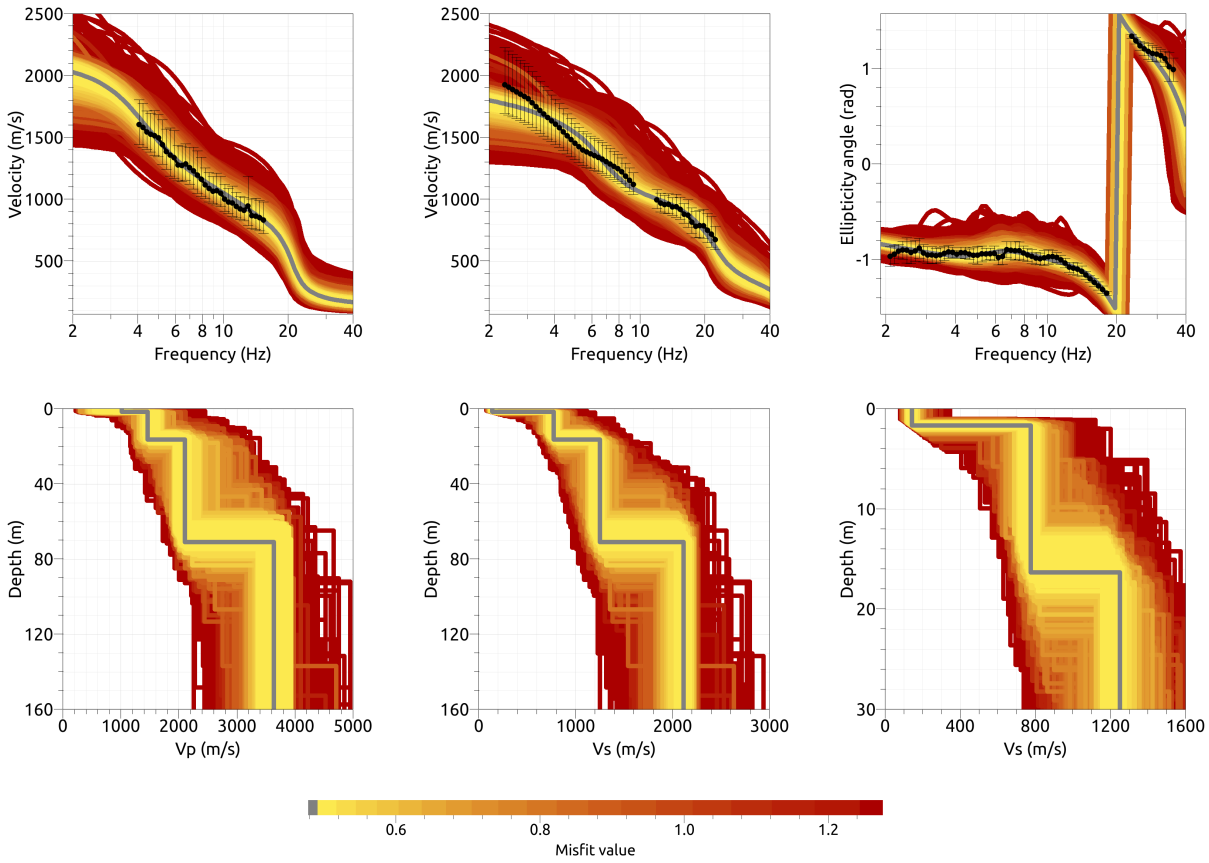

Figure 17: Inversion SZWD4l2. Top line: Dispersion curves for Love waves (left) and Rayleigh waves (center) and Rayleigh wave ellipticity angle (right) of the respective fundamental modes. Bottom line: P-wave velocity profiles (left), S-wave velocity profiles (center and zoom on the right). The black dots indicate the data points used for the inversion, the gray line indicates the best-fitting model.

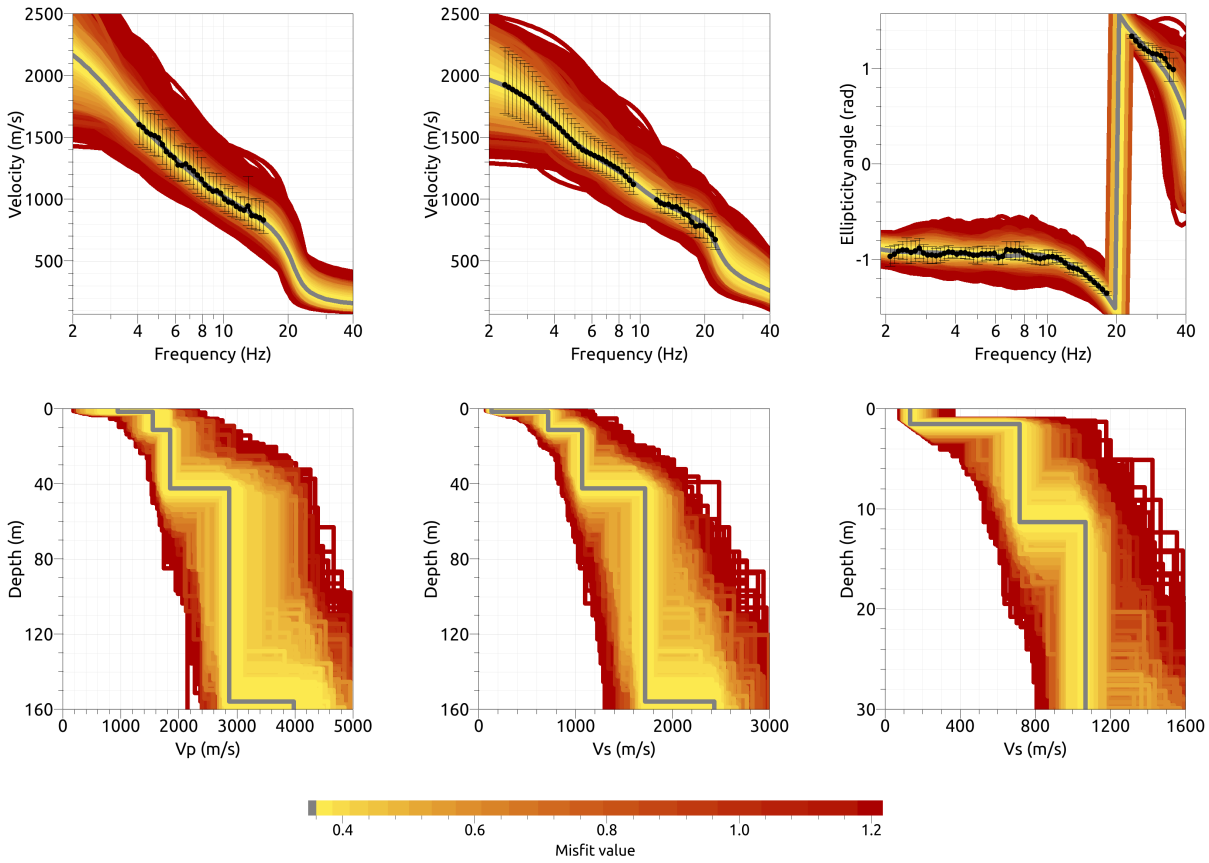

Figure 18: Inversion SZWD5l2. Top line: Dispersion curves for Love waves (left) and Rayleigh waves (center) and Rayleigh wave ellipticity angle (right) of the respective fundamental modes. Bottom line: P-wave velocity profiles (left), S-wave velocity profiles (center and zoom on the right). The black dots indicate the data points used for the inversion, the gray line indicates the best-fitting model.

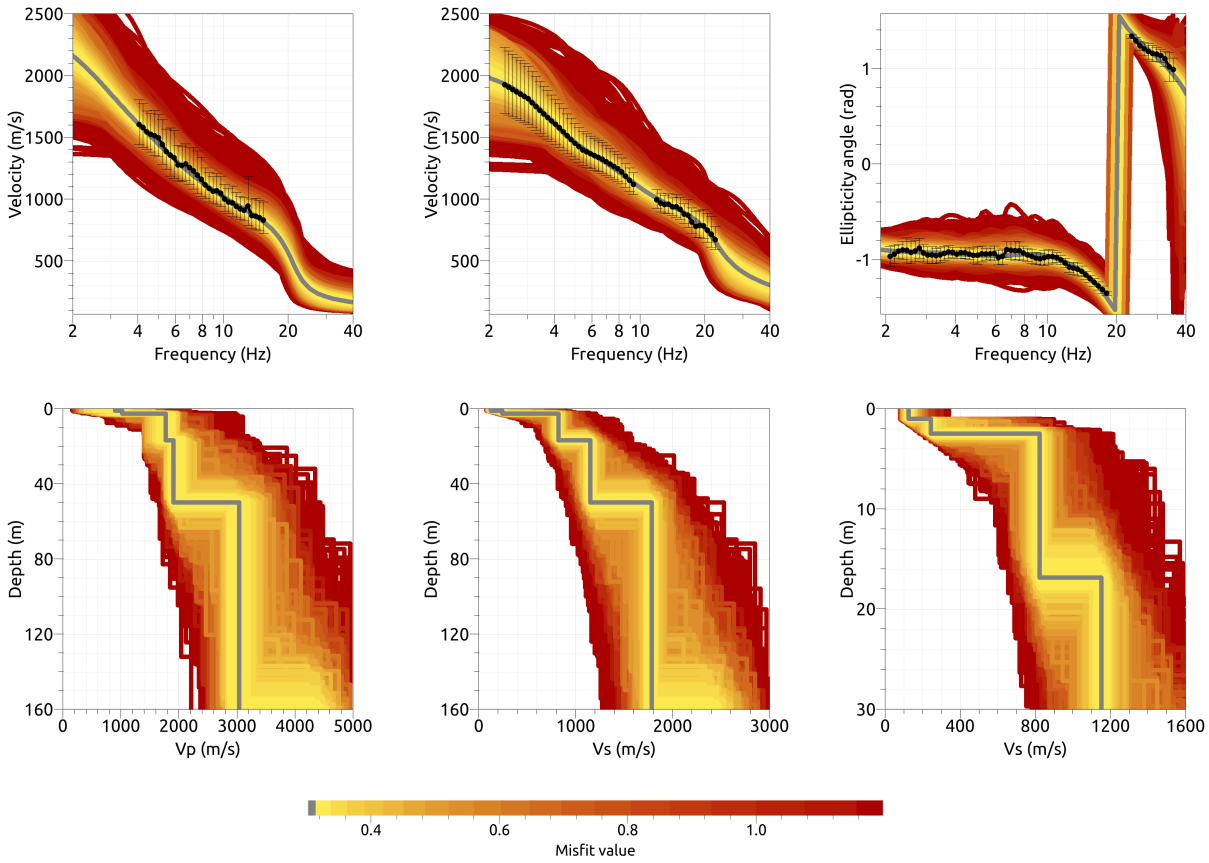

Figure 19: Inversion SZWD6l2. Top line: Dispersion curves for Love waves (left) and Rayleigh waves (center) and Rayleigh wave ellipticity angle (right) of the respective fundamental modes. Bottom line: P-wave velocity profiles (left), S-wave velocity profiles (center and zoom on the right). The black dots indicate the data points used for the inversion, the gray line indicates the best-fitting model.

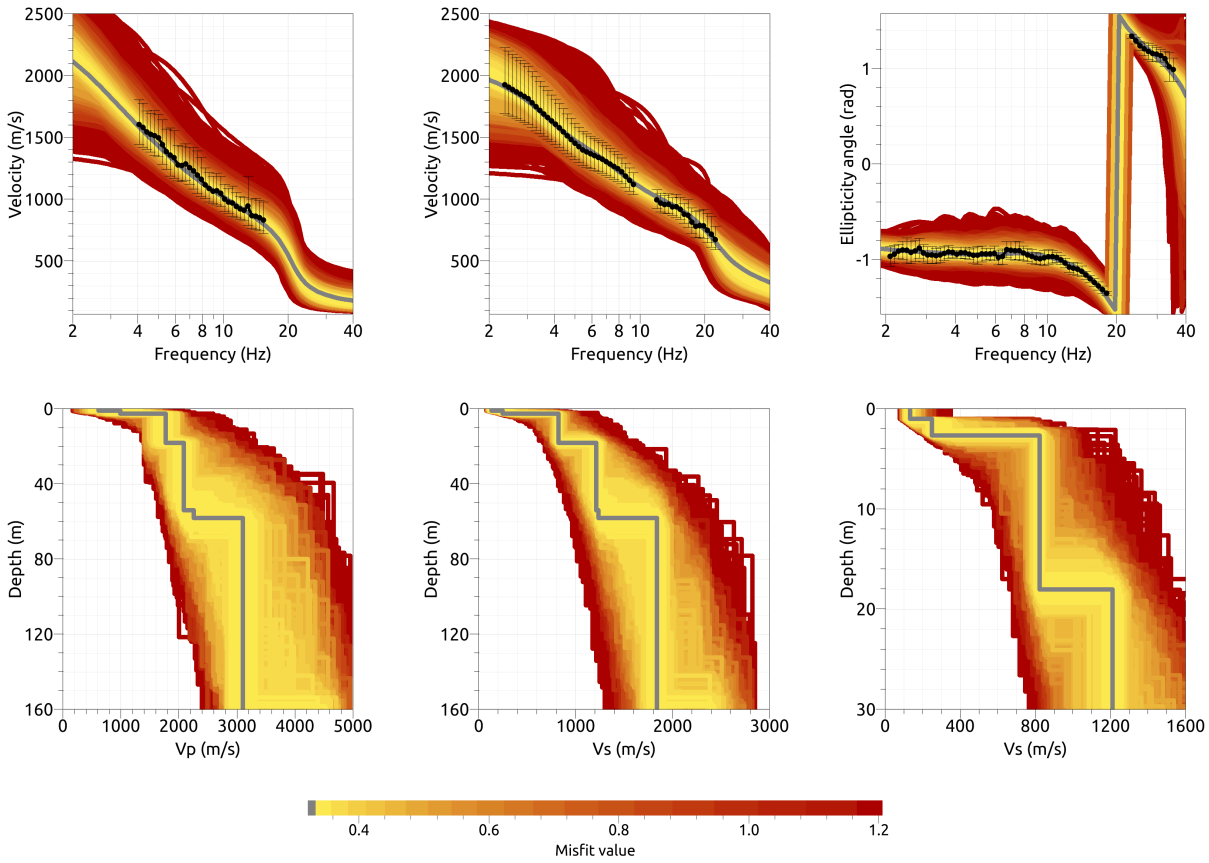

Figure 20: Inversion SZWD7l2. Top line: Dispersion curves for Love waves (left) and Rayleigh waves (center) and Rayleigh wave ellipticity angle (right) of the respective fundamental modes. Bottom line: P-wave velocity profiles (left), S-wave velocity profiles (center and zoom on the right). The black dots indicate the data points used for the inversion, the gray line indicates the best-fitting model.

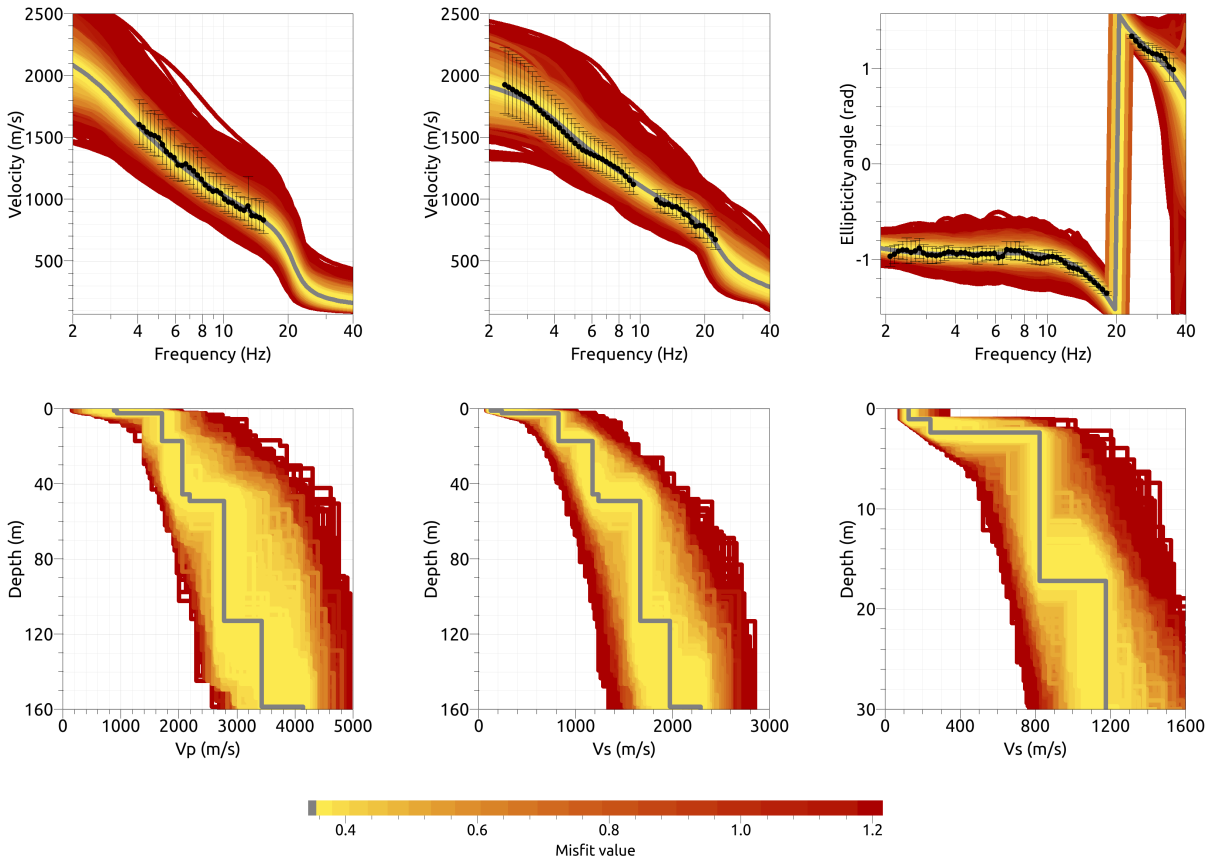

Figure 21: Inversion SZWD8l2. Top line: Dispersion curves for Love waves (left) and Rayleigh waves (center) and Rayleigh wave ellipticity angle (right) of the respective fundamental modes. Bottom line: P-wave velocity profiles (left), S-wave velocity profiles (center and zoom on the right). The black dots indicate the data points used for the inversion, the gray line indicates the best-fitting model.

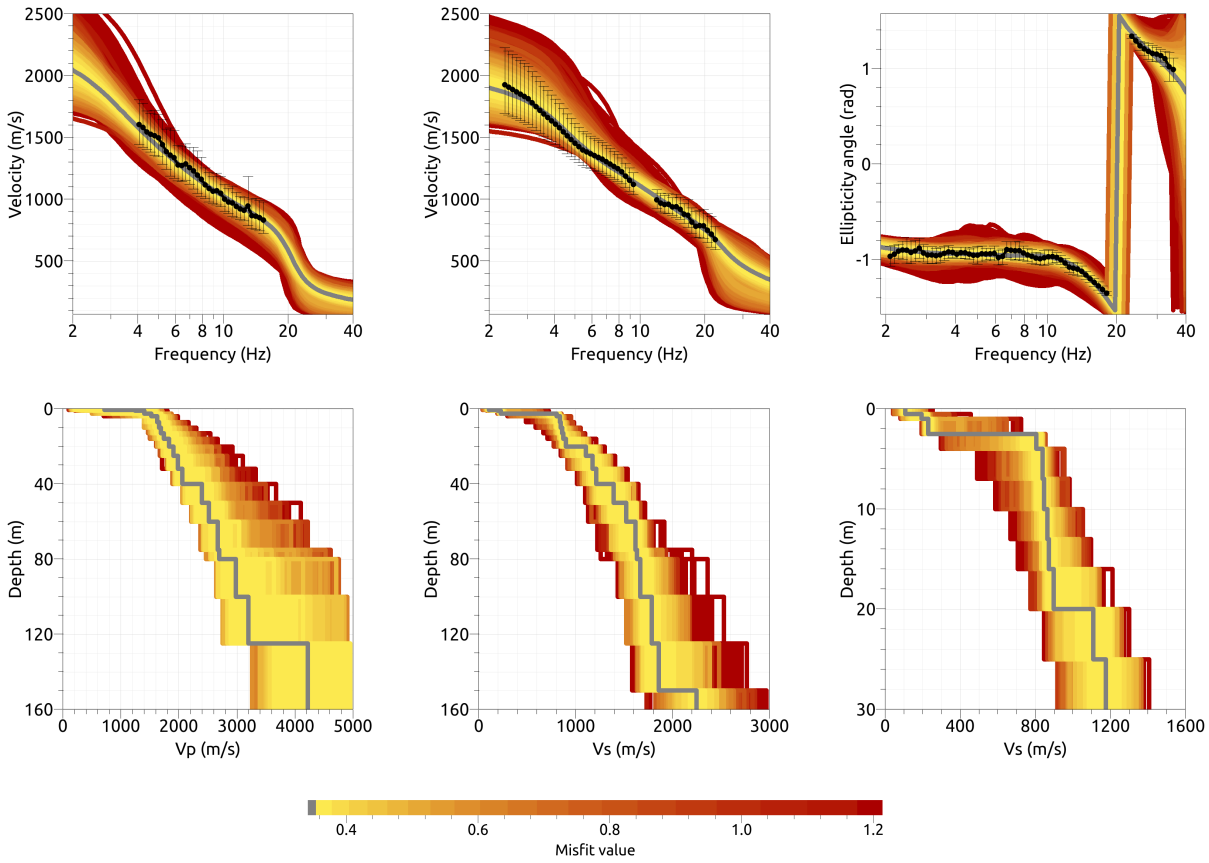

Figure 22: Inversion SZWDfix2. Top line: Dispersion curves for Love waves (left) and Rayleigh waves (center) and Rayleigh wave ellipticity angle (right) of the respective fundamental modes. Bottom line: P-wave velocity profiles (left), S-wave velocity profiles (center and zoom on the right). The black dots indicate the data points used for the inversion, the gray line indicates the best-fitting model.

4.4 Overview of the inversion result

The S-wave velocity profiles of the best-fitting models of all inversions are shown in Fig. 23. The inversions using targets 1 and 2 give very similar results, especially in the superficial 100 m. This is not surprising as both targets only differ in the low-frequency part. Apart from the superficial layers, the inversions do not show clear interfaces at depth and a more gradual increase of velocity. The 4-layer and 5-layer inversions differ from the other inversions and will be discarded for the further analysis.
The more complex models have a superficial layer with a shear-wave velocity of about 130 m/s and a thickness of about 1 m, followed by a second layer with a velocity of about 245 m/s down to about 2.5 m, where the velocity already increases to over 800 m/s. Below, the S-wave velocity increases gradually and reaches between 2200 and 2500 m/s at 200 m depth.
The V_{S30} values for the inversions with at least six layers range from 695.4 to 704.5 m/s (average value $700.3 \pm 4.1\ m/s$). This corresponds to soil class B in both EC8 and SIA261.

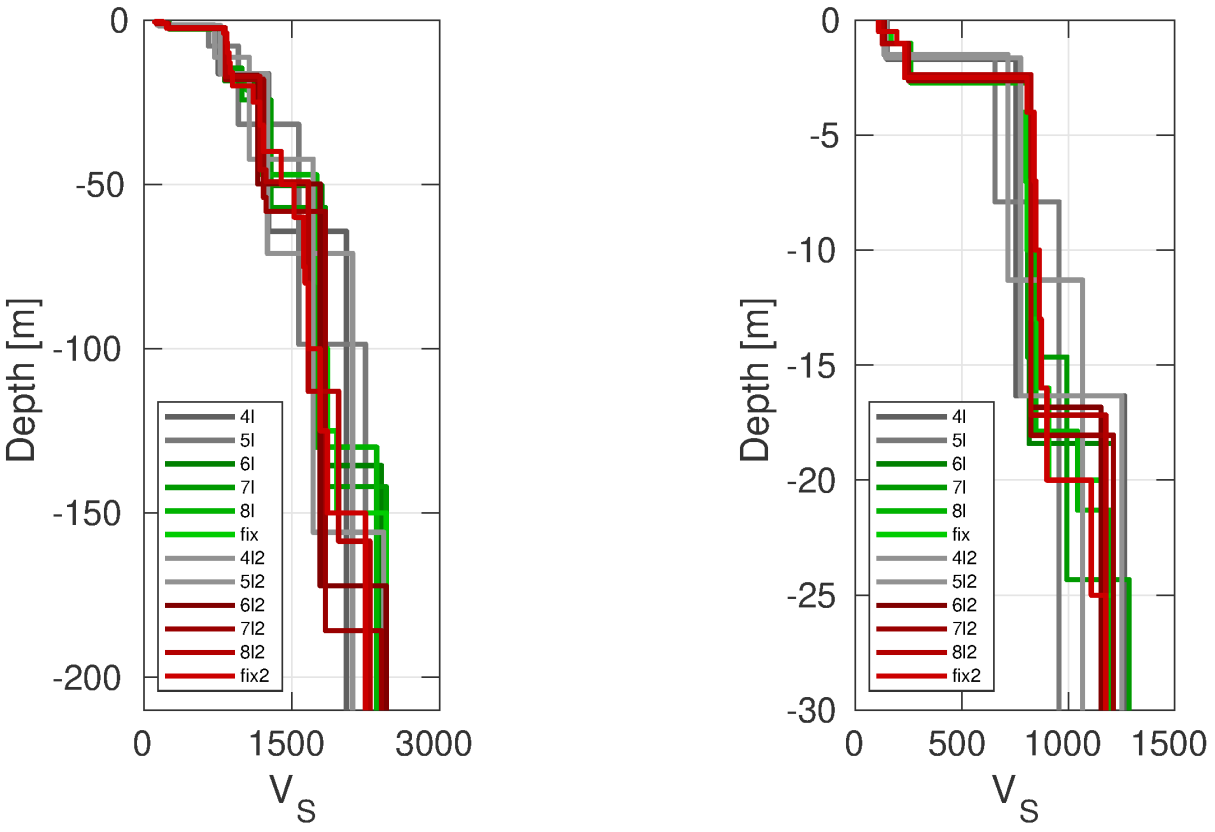

Figure 23: Overview of shear-wave velocity profiles of the best-fitting models of all inversions (left) and a zoom on the shallow part for the inversions (right).

4.5 Amplification function

In Fig. 24, the theoretical amplification function for the best models with at least six layers resulting from the inversions is compared with the empirical amplification of station SZWD2, based on 47 events so far. The empirical amplification shows a first peak below 1 Hz, which is not modeled by the inversion results, as such low frequencies had not been used for the inversion. In the range from about 2 to 15 Hz, the empirical amplification shows a slight increase with frequency, but without pronounced peaks. It shows a strong peak just below 20 Hz. The modeled amplification from the inversions is close in the upgoing trend and shows a strong peak just above 20 Hz. The values are in general also higher than the empirical amplification, but give a good qualitative result.

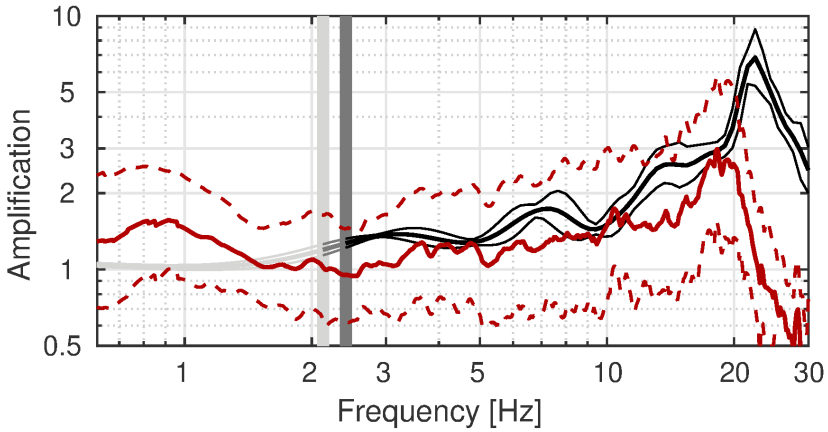

Figure 24: Comparison between the modeled amplification for the final set of best models of the different inversions (in grey to black, with standard deviation) and the empirical amplification measured at station SZWD2 (red, with standard deviation) for all inversions using at least six layers for targets 1 and 2. The vertical light and dark grey bars correspond to the lowest frequency of the ellipticity and dispersion curves used for the inversion, respectively.

4.6 Quarter-wavelength representation

The quarter-wavelength velocity approach (Joyner et al., 1981) provides, for a given frequency, the average velocity at a depth corresponding to 1/4 of the wavelength of interest. It is useful to identify the frequency limits of the experimental data (the minimum frequency of the dispersion curve used in the inversions is 4.06 Hz for target 1 and 2.37 Hz for target 2, the minimum frequency used for the ellipticity inversion 2.09 Hz). The results using this proxy show that the dispersion curves constrain the profiles down to about 164 m maximum (Fig. 25). Moreover, the quarter wavelength impedance-contrast introduced by Poggi et al. (2012) is also displayed in the figure. It corresponds to the ratio between two quarter-wavelength average velocities, respectively from the top and the bottom part of the velocity profile, at a given frequency (Poggi et al., 2012). This curve shows a strong contrast at the fundamental frequency of the site.

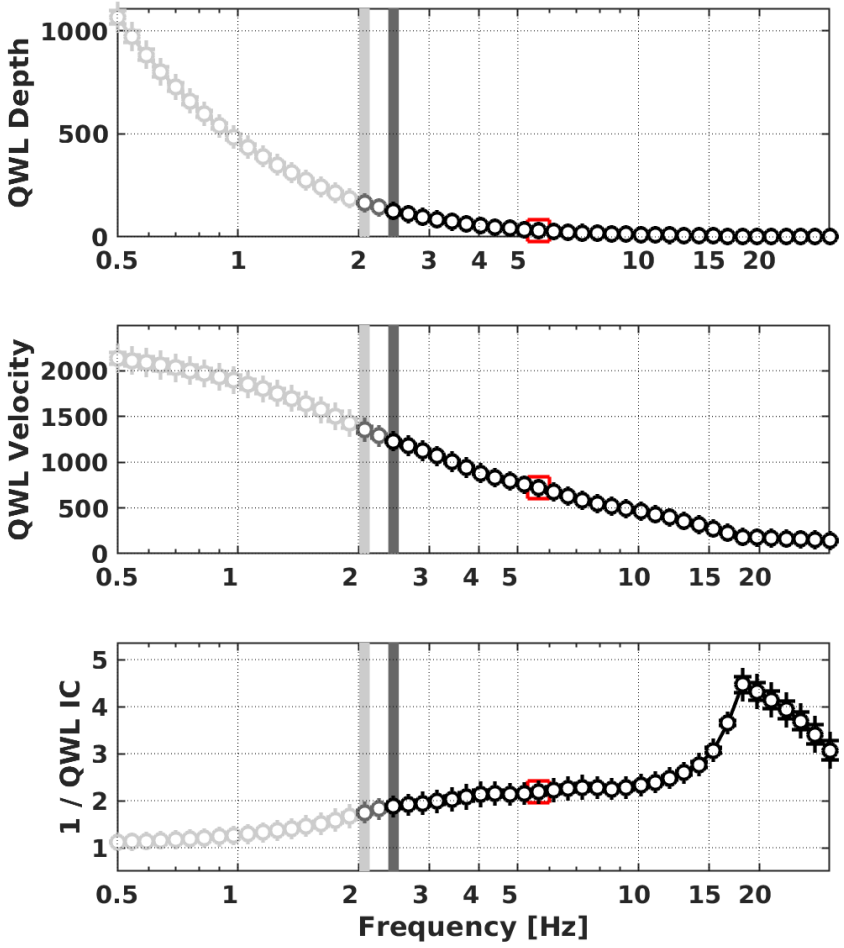

Figure 25: Quarter wavelength representation of the velocity profile for the best models of the inversions with at least six layers for targets 1 and 2 (top: depth, center: velocity, bottom: inverse of the impedance contrast). The black curves are constrained by the dispersion curves, the light grey curves are not constrained by the data. The red square corresponds to V_{S30}.

5 Conclusion

We performed a passive array measurement to characterize the soil underneath station SZWD2 in Zweisimmen (BE). According to the geological atlas, the station is located on moraine.
The dispersion curves for Love and Rayleigh waves could be measured over a wide frequency range, from around 4.1 to 15.4 Hz for Love waves and from 2.4 to 22.4 Hz for Rayleigh waves, but the mode attribution for Rayleigh waves is not straightforward. In the H/V and ellipticity curves, a strong peak is present throughout the array, but at variable frequencies ranging from about 4 to over 30 Hz. At the location of the permanent station SZWD2, this peak is found at about 20 Hz. We assume that this peak is caused by a shallow layer of low seismic velocity and variable thickness throughout the area.
Joint inversions with two different targets were performed, using different parts of the Rayleigh wave dispersion curves at low frequencies. The results were, however, very similar. The final models show two superficial layers, the first with a thickness of about 1 m and an S-wave velocity of 130 m/s, the second down to about 2.5 m with a velocity of 245 m/s. At this depth, the velocity already reaches values of over 800 m/s and increases gradually to over 2200 m/s at about 200 m depth. The V_{S30} of the final models is about 700 m/s, corresponding to soil class B in both EC8 and SIA261.

Acknowledgements

The authors thank Sanjay Bora, Dario Chieppa, and Simon Rouwendaal for their help during the array measurements.

References

Aki, K. (1957). Space and time spectra of stationary stochastic waves, with special reference to microtremors. *Bull. Earthquake Res. Inst. Tokyo Univ.*, 35:415–456.

Bettig, B., Bard, P.-Y., Scherbaum, F., Riepl, J., Cotton, F., Cornou, C., and Hatzfeld, D. (2001). Analysis of dense array noise measurements using the modified spatial auto-correlation method (SPAC): application to the Grenoble area. *Boll. Geof. Teor. Appl.*, 42:281–304.

Burjánek, J., Gassner-Stamm, G., Poggi, V., Moore, J. R., and Fäh, D. (2010). Ambient vibration analysis of an unstable mountain slope. *Geophys. J. Int.*, 180:820–828.

Burjánek, J., Moore, J. R., Molina, F. X. Y., and Fäh, D. (2012). Instrumental evidence of normal mode rock slope vibration. *Geophys. J. Int.*, 188:559–569.

Fäh, D., Wathelet, M., Kristekova, M., Havenith, H., Endrun, B., Stamm, G., Poggi, V., Burjanek, J., and Cornou, C. (2009). Using ellipticity information for site characterisation. NERIES deliverable JRA4 D4, available at http://www.neries-eu.org.

Hobiger, M., Bard, P.-Y., Cornou, C., and Le Bihan, N. (2009). Single station determination of Rayleigh wave ellipticity by using the random decrement technique (RayDec). *Geophys. Res. Lett.*, 36.

Joyner, W. B., Warrick, R. E., and Fumal, T. E. (1981). The effect of Quaternary alluvium on strong ground motion in the Coyote Lake, California, earthquake of 1979. *Bull. Seismol. Soc. Am.*, 71(4):1333–1349.

Maranò, S., Reller, C., Loeliger, H.-A., and Fäh, D. (2012). Seismic waves estimation and wavefield decomposition: Application to ambient vibrations. *Geophys. J. Int.*, 191:175–188.

Poggi, V., Edwards, B., and Fäh, D. (2012). Characterizing the Vertical-to-Horizontal ratio of ground motion at soft-sediment sites. *Bull. Seismol. Soc. Am.*, 102(6):2741–2756.

Poggi, V. and Fäh, D. (2010). Estimating Rayleigh wave particle motion from three-component array analysis of ambient vibrations. *Geophys. J. Int.*, 180:251–267.

Wathelet, M., Jongmans, D., and Ohrnberger, M. (2005). Direct inversion of spatial autocorrelation curves with the neighborhood algorithm. *Bull. Seismol. Soc. Am.*, 95:1787–1800.